Analytical Methods

Accepted Manuscript

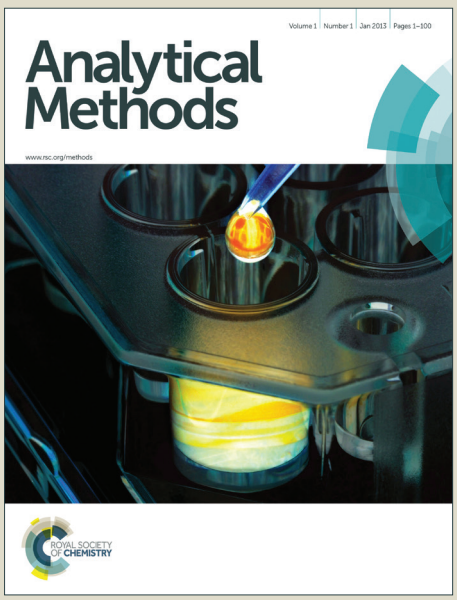

This is an *Accepted Manuscript*, which has been through the Royal Society of Chemistry peer review process and has been accepted for publication.

Accepted Manuscripts are published online shortly after acceptance, before technical editing, formatting and proof reading. Using this free service, authors can make their results available to the community, in citable form, before we publish the edited article. We will replace this *Accepted Manuscript* with the edited and formatted *Advance Article* as soon as it is available.

You can find more information about *Accepted Manuscripts* in the Information for Authors.

ROYAL SOCIETY OF CHEMISTRY

www.rsc.org/methods

Graphic Abstract

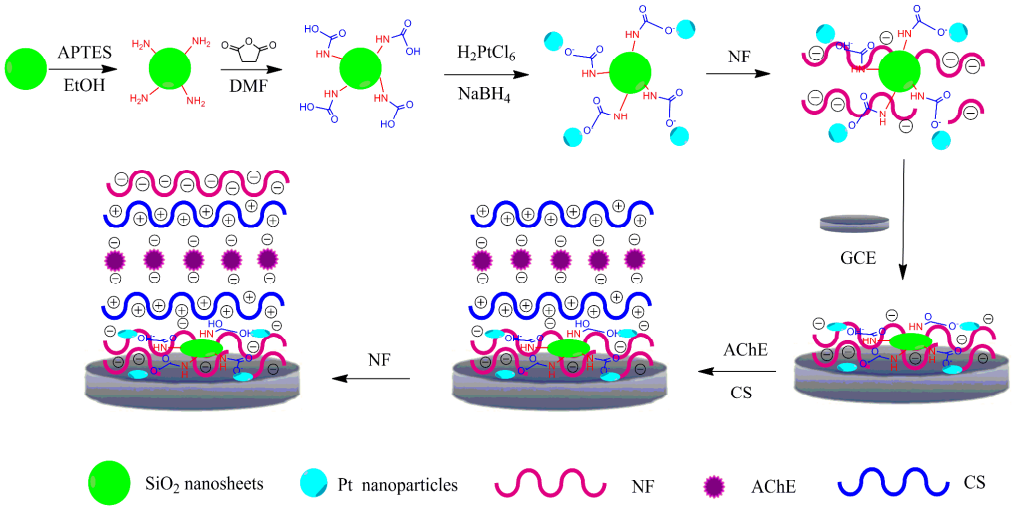

Title page

Carboxylic silica nanosheets-platinum nanoparticles modified glass carbon electrode for pesticides detection

Can-Peng Li [a]*, Shuangmei Fan [a], Chunyan Yin [a], Nan Zhang [a], Sie Du [a], Hui Zhao [b]*

[a] School of Chemical Science and Engineering, Yunnan University, Kunming 650091, China

[b] Laboratory for Conservation and Utilization of Bio-resource, Yunnan University, Kunming 650091, China

*Corresponding author

Phone/fax: +86-871-65031119.

E-mail: lcppp1974@sina.com (C.-P. Li); zhaohyau@yahoo.com.cn (H. Zhao)

2 North Cuihu Road

Kunming 650091

P. R. China

24 December, 2013

Abstract: Silica nanosheets were prepared from montmorillonite and carboxyl functionalized by a chemical method. Platinum nanoparticles (Pt NPs) were also synthesized on carboxylic silica nanosheets (CSNS). An acetylcholinesterase (AChE) biosensor based on a Pt NPs, CSNS, and Nafion nanocomposite-modified glass carbon electrode was successfully developed. The AChE biosensor showed favorable affinity to acetylthiocholine chloride (ATCl) and catalyzed the hydrolysis of ATCl with an apparent Michaelis–Menten constant value of 125 μM. Under optimal conditions, the biosensor detected methyl parathion and carbaryl in the range of 1.0×10^{-12} M–1×10^{-8} M. The detection limits for methyl parathion and carbaryl were 5.52×10^{-13} and 5.65×10^{-13} M, respectively. The developed biosensor was inexpensive and exhibited good sensitivity, stability, and reproducibility, thus providing a promising tool for the analysis of enzyme inhibitors. A simple and effective immobilization platform was also provided for effectively immobilizing the enzyme on the electrode surface.

Keywords: carboxylic silica nanosheets; platinum nanoparticles; acetylcholinesterase biosensor; pesticides

1. Introduction

The extensive use of pesticides for pest control has raised serious public concern regarding health, environment, and food safety in modern agriculture. Pesticides

exhibit acute toxicity. The inhibition of acetylcholinesterase (AChE) activity by carbamate and organophosphorus pesticides can disturb normal neuronal functions and even cause death.[1–3] Measurement of pesticides in water and food is thus of great importance.

Existing methods for pesticides monitoring include various chromatographic techniques. These techniques have reasonably low limits of detection and are very selective, but they require time, solvent-consuming sample pretreatment, expensive equipment, and highly trained personnel. Over the last decade, the use of enzymatic biosensors based on immobilizing bioactive enzymes and related materials has become an attractive and popular focus for scientific research. The rapid response, high sensitivity, and intrinsic selectivity of biosensors have rendered them usable in many potential applications in various fields, including medical diagnostics, pharmaceuticals, and environmental control. Among the enzyme biosensors currently available, the AChE biosensor has gained considerable attention because of its favorable properties, which include simplicity, rapidity, reliability, and low-cost instrumentation.[4–7] Although this method can't selectively detect and quantify different pesticides because most organophosphorus and carbamate pesticides can inactivate cholinesterase, it is suitable as a screening tool for providing a rapid response and signalling the existence of contaminated samples.

The nano-silica discovered by scientists at the Mobil Corporation in 1992 was quickly recognized as a breakthrough that could lead to a variety of important applications.[8] Nano-silica has excellent properties, such as large surface area coverage,

biocompatibility, non-toxicity, high ionic conductivity, and chemical and thermal stability, all of which make the material ideal as a support for adsorption processes, catalysis, chemical separation, nano-devices, electrochemical sensors, and biosensors.[9] Silica nanomaterials are a class of important catalysts and adsorbents that allow the rapid transport of bulky molecules and promote improved performance in petrochemical and biomass processing. Zhang et al.[10] synthesized self-pillared zeolite nanosheets with excellent catalytic and adsorption properties. Kaushik et al.[9] used bovine serum albumin, rabbit-immunoglobulin antibodies, chitosan (CS), and fumed silica nanoparticles (NPs) to modify indium-tin oxide glass immunoelectrode for ochratoxin detection with improved sensing characteristics. Abdullah et al.[11] reported the immobilization of 3-methylbenzothiazolone hydrazone in Nafion (NF)/sol-gel silicate and horseradish peroxidase in CS for the determination of phenolic compounds with good sensitivity, reproducibility, and stability. Zhang et al.[12] reported the use of enzyme electrodes manufactured based on neutral red-doped silica nanoparticles for detection of glucose, lactate, L-glutamate, and hypoxanthine. Therefore, exploration of the properties of silica nanomaterials for application in biosensors has considerable scope. However, because of several inherent disadvantages, such as their brittleness, low hydrophilicity, and relatively poor biocompatibility, silica nanomaterials must be modified to meet most application requirements. In this regard, carboxyl (–COOH) grafting in silica nanomaterials can improve the hydrophilicity of the resultant nanomaterials, and the developed hydrophilicity may be expected to promote enzymatic catalytic reactions. Therefore,

silica nanomaterials with a carboxyl group in their structures are expected to show improved affinity toward enzymes.

Platinum NPs (Pt NPs) and functionalized silica nanohybrids are nanocomposites that successfully integrate the unique properties of two classes of materials and exhibit new functions by the cooperative effects of Pt NPs and functionalized nano-silica. In these nanocomposites, Pt NPs are usually anchored to the surface of functionalized silica. Existing research results indicate that Pt NPs and functionalized silica nanohybrids modified glass carbon electrode (GCE) show high electron mobility, catalytic activity, and sensitivity. Yang et al.[13] showed that a glucose biosensor based on nano-SiO_2 and "unprotected" Pt nanoclusters demonstrates high sensitivity and good stability. Zou et al.[14] reported that a biosensor based on electrodeposition of Pt NPs on carbon nanotubes and immobilizing enzyme with chitosan-silica sol-gel shows excellent electrocatalytic activity and high stability. Carboxylic silica nanosheets (CSNS) with a carboxyl functional group can be bound with Pt NPs, and Pt NPs can be uniformly separated on CSNS. Pt NPs have also been reported to provide immobilization sites for the enzymes due to their excellent conductive property and compatibility.[15,16] Thus, the cooperative effects between Pt NPs and CSNS may enhance the performance of the Pt NPs–CSNS nanocomposites.

NF polymer is chemically and thermally inert, nonelectroactive, hydrophilic, and insoluble in water, thus possessing almost ideal properties for preparation of modified electrodes.[17] Some nanomaterials with high conductivity and catalytic activity may be combined with NF and used to modify electrodes and achieve improved sensitivity,

selectivity, and stability. Kumaravel et al.[18] described a nanosilver/NF electrode for the electrochemical detection of methyl parathion with strong electrocatalytic activity, good stability, and reproducibility. Li et al.[19] presented a NF-graphene nanocomposite film modified electrode for the sensitive determination of cadmium. Li et al.[20] described a horseradish peroxidase biosensor based on NF/graphene with good operational storage and storage stability for the determination of H_2O_2. CS is an abundant natural biopolymer with excellent film forming ability, biocompatibility, and non-toxicity. CS provides a natural microenvironment for the enzyme as well as sufficient accessibility for electrons to shuttle between the enzyme and the electrode.[21] Thus, NF and CS can be used to improve the performance of AChE biosensors.

In this work, a sensitive and stable AChE biosensor is developed using a simple, rapid, and economical approach for the detection of pesticides. Pt NPs, CSNS, and NF were utilized to construct an AChE biosensor based on Pt NPs–CSNS–NF/GCE. The performance of the developed biosensor was investigated in detail, and methyl parathion and carbaryl were determined in real samples using the proposed AChE biosensor.

2. Experimental

2.1 Reagents and Apparatus

Acetylthiocholine chloride (ATCl), AChE (Type C3389, 500 U/mg from electric eel),

CS (85% deacetylation), 3-Aminopropyltriethoxysilane (APTES, 99%), N, N-dimethylformamide (DMF), pyridine 2-aldoxime methiodide (PAM), succinic anhydride, and NF (5% in lower aliphatic alcohols and water) were purchased from Sigma-Aldrich (St. Louis, USA). Methyl parathion and carbaryl (purity 99.99 %) were obtained from the Institute of Environmental Protection of China's Agriculture Ministry (Beijing, China). The montmorillonite was purchased from Beaufour Ipsen Pharmaceutical (Tianjin, China). $H_2PtCl_6 \cdot 6H_2O$ was obtained from Shanghai Chemical Reagent Company (Shanghai, China). All other reagents were of analytical grade. Aqueous solutions were prepared with deionized water (DW).

The electrochemical measurements were carried out on an IM6ex electrochemical workstation (Zahner Elektrik Instruments, Germany). A conventional three-electrode system was employed with a saturated calomel electrode (SCE) as the reference electrode, a platinum foil as the counter electrode, and the modified GCE (diameter=3mm) as the working electrodes. Cyclic voltammetry (CV) and differential pulse voltammetry (DPV) measurements were performed in 0.1M phosphate buffer (PBS, pH 7.4). DPV was performed from 0.25 to 0.80 V with the parameters of increment potential, 0.004 V; pulse amplitude, 0.05 V; pulse width, 0.05 s; sample width, 0.0167 s; pulse period, 0.2 s and quiet time, 2 s. All experiments were performed at room temperature (25±1 ^{o}C). CSNS were characterized by Fourier transform infrared spectrometry (FTIR, Thermo Fisher SCIENTIFIC Nicolet IS10 USA), Pt NPs–CSNS nanocomposites were characterized by scanning electron microscopy (SEM, QUNT200 USA) and X-ray diffractometer (XRD, Rigaku TTRⅢ,

Japan).

2.2 Preparation of CSNS

Silica nanosheets (SNS) were prepared from montmorillonite. The process of preparation of SNS was supplied in **Supplementary Materials**. SNS was amino-functionalized as follows: 250 mg of SNS was dispersed in 20 ml of ethanol, and then 2.5 ml of APTES was added to the dispersion with a vigorously stirring. After stirred overnight, the resulting mixture were cleaned with ethanol for several cycles and redispersed in DMF. SNS-NH_2 was obtained. SNS was carboxyl-functionalized as previously reported[22] with the modification of replacing method of drying in an oven with vacuum freeze-drying. Briefly, a dispersion of SNS-NH_2 obtained in DMF (20 ml) was added dropwise to a flask containing 20 ml of 0.1 M succinic anhydride in DMF. The mixture was stirred for 24 h; the resulting SNS with carboxylic-function groups at their surface (SiO_2-COOH) were cleaned with DMF for several cycles. After vacuum freeze-drying, CSNS was obtained.

2.3 Synthesis of Pt NPs–CSNS nanocomposites

The Pt NPs–CSNS nanocomposites were prepared as follows: 2.0 mg CSNS were suspended in 2.0 ml of 0.45 mM H_2PtCl_6 aqueous solution. Then 5.0 ml pyridine and 1.0 ml of 0.01 M sodium citrate were added to the above suspension by sonicating for

10 min disperse CSNS equably. Ice-cold, freshly prepared 1.0 ml of 0.01 M $NaBH_4$ solution was added to the above mixture while stirring until the color of the solution did not change. After stirring for an additional 10 h, the suspension was separated by centrifuging at 12,000 rpm for 20 min, washed with DI water for several cycles. After vacuum freeze-drying, Pt NPs–CSNS nanocomposites were obtained.

2.4 Preparation of AChE biosensor

NF solution (0.125%, W/V) was prepared by diluting 5% of NF with ethanol and DI water (V/V, 1/1). The Pt NPs–CSNS (0.5 mg) were added to 1.0 ml of NF solution and sonicated thoroughly until a homogeneous suspension of Pt NPs–CSNS–NF was obtained. Similarly, 0.5 mg/ml CSNS–NF and SNS–NF homogeneous suspensions were obtained and stored at 4 □.

A GCE was polished carefully to a mirror-like with 0.3 and 0.05 μm alumina slurry and sequentially sonicated for 3 min in ethanol and water. Before the experiment, the electrode was scanned from -0.1 to +1.1V until a steady-state current-voltage curve was obtained. The Pt NPs–CSNS–NF/GCE was prepared by casting 5 μl of the 0.5 mg/ml Pt NPs–CSNS–NF suspension onto the GCE and drying at room temperature. A similar casting procedure was used to prepare NF/GCE, SNS–NF/GCE and CSNS-NF/GCE. The AChE–CS solution contained 0.05 U AChE and 0.2% CS (W/V). The electrodes obtained were finally coated with 4.5 μl AChE–CS (V/V, 2:1) solutions and dried overnight at 4□. The modified electrodes

were washed with pH 7.4 PBS to remove the unbound AChE. Finally, AChE–CS/NF/GCE, AChE–CS/SNS–NF/GCE, AChE–CS/CSNS–NF/GCE, and AChE–CS/Pt NPs–CSNS–NF/GCE biosensors were each covered with 3 μl 0.1% (W/V) NF as the protective membrane and then stored at 4 ^{o}C NF/AChE–CS/GCE was also produced as a control. The process of preparation Pt NPs–CSNS nanocomposite and fabrication of the AChE biosensor were showed in **Scheme 1**.

2.5 Detection of ATCl

CV measurements were performed in 0.1 M PBS between 0.0 and 1.0 V for characteristic investigations of NF/AChE–CS/Pt NPs–CGR–NF/GCE biosensors. The apparent Michaelis-Menten constant (K_m^{app}) of the biosensor was calculated from the Line weaver-Burk equation:

$$\frac{1}{i_{ss}} = \left(\frac{K_m^{app}}{i_{max}}\right)\cdot\left(\frac{1}{C}\right) + \left(\frac{1}{i_{max}}\right) \qquad (1)$$

where i_{ss} is the steady-state current after the addition of substrate, i_{max} is the maximum current measured under saturated substrate condition and C is the concentration of the substrate. The K_m^{app} value which gives an indication of the enzyme substrate kinetics for the biosensor was determined by analysis of the slope and intercept of the plot of the reciprocals of steady-state current versus ATCl concentration.

2.6 Effect of incubation time

Inhibition of methyl parathion and carbaryl were tested by CV in terms of their effect on AChE activity at different incubation time (2 to 16 min) in a pesticide solution (10^{-9} M), respectively.

2.7 Detection of pesticides

The NF/AChE–CS/Pt NPs–CSNS–NF/GCE was first immersed in pH 7.4 PBS containing different concentrations of standard pesticide at 25±1 ^{o}C for 10 min and then transferred to the electrochemical cell of pH 7.4 PBS containing 0.5 mM ATCl to study the amperometric response by DPV between 0.25 and 0.80 V. The inhibition of pesticide was calculated as follows:

$$\text{inhibition} \quad (\%) = \frac{i_{\text{P,control}} - i_{\text{P,exp}}}{i_{\text{P,control}}} \times 100\% \qquad (2)$$

where $i_{\text{p,control}}$ and $i_{\text{p,exp}}$ are the peak currents of ATCl on the biosensor in the absence and presence of pesticide inhibition, respectively.

The detection limit (LD) was calculated by using the equation given below:

$$LD = 3S/b \qquad (3)$$

where S is the standard deviation of the blank solution, b is the slope of the analytical curve.

2.8 Interference study

The species of glucose (0.5 mM), citric acid (0.5 mM), oxalic acid (0.5 mM), PO_4^{3-}

(0.5 mM), SO_4^{2-} (0.5 mM), NO_3^- (0.5 mM), 0.5 mM p-nitrophenol, 0.5 mM nitrobenzene, 0.5 mM p-nitroaniline, 0.5 mM trinitrotoluene, 0.5 mM toluene, and 0.5 mM p-toluenesulfonic acid that may interfere the determination were studied. Other pesticides such as malathion, acephate, chlorpyrifos, and carbofuran were also used to study the interference between the various kinds of pesticides. The signal for a 0.5 mM ATCl was compared with the signal obtained in the presence of the interfering species after incubated by 10^{-9} M methyl parathion for 10 min.

2.9 Precision of measurements and stability studies

The intra-assay precision of the biosensor was evaluated by testing one NF/AChE–CS/Pt NPs–CSNS–NF/GCE for six times in 0.5 mM ATCl after being immersed in the 1.0×10^{-10} M methyl parathion for 10 min. The inter-assay precision was estimated with six different biosensors in the same way. The relative standard deviation (RSD) of intra-assay and inter-assay were demonstrated reproducibility of the biosensor. Stability was evaluated by testing the current response of the NF/AChE–CS/Pt NPs–CSNS –NF/GCE biosensor in 0.1 M PBS containing 0.5 mM ATCl by CV every five days. The retained ratio of its initial current response was indicated the stability of biosensor.

2.10 Preparation and analysis of real samples

Two samples, tap water sample and water sample from natural lake, were filtered through a 0.22 μm membrane and the pH was adjusted to 7.4. Apple and cabbage samples were obtained from a local market in Kunming City. After simple pretreatment, different concentrations of methyl parathion and carbaryl were added to study the recovery under the optimal conditions.

3. Results and discussion

3.1 Characterization of CSNS and Pt NPs–CSNS

The SEM image in **Fig. 1A** reveals a SNS consisting of random aggregates of thin sheets approximately 10 nm thick. The SEM image in **Fig. 1B** shows a synthesized Pt NPs–CSNS nanocomposite. In this image, CSNS was uniformly covered by the Pt NPs.

The FTIR spectrum of SNS (**Fig. 1C**, **blank line**) displays the presence of Si–O–Si (1097 cm^{-1}), Si–O (797 cm^{-1} and 472 cm^{-1}), -OH (3450 cm^{-1}), and H–O–H (1630 cm^{-1}). Compared with that of SNS, the FTIR spectrum of CSNS (**Fig. 1C**, **red line**) displays the presence of C=O (1722 cm^{-1}). Strong peak at 1722 cm^{-1} confirm the presence of a carboxyl group, which indicates the successful functionalization of SNS with carboxyl groups.

Fig. 1D shows the XRD patterns of CSNS (**blank line**) and the Pt NPs–CSNS (**red line**) nanocomposites. Well-defined peaks are observed at 21.74^{o}, 22.17^{o}, 26.66^{o},

27.67°, and 35.89° (2θ), which is consistent with the standard pattern for orthorhombic SiO_2 (JSPDS 00-050-1432). Well-defined peaks are also found at 39.76°, 46.24°, and 67.29° (2θ), which indicates the formation of the cubic phase of Pt NPs. The XRD patterns show that Pt NPs have been synthesized on the surface of CSNS.

3.2 Electrochemical behavior of the NF/AChE–CS/Pt NPs–CSNS–NF/GCE

CV experiments with ATCl and the enzymatic product thiocholine were conducted on the NF/AChE–CS/GCE, NF/AChE–CS/NF/GCE, NF/AChE–CS/SNS–NF/GCE, NF/AChE–CS/CSNS–NF/GCE, and NF/AChE–CS/Pt NPs–CSNS–NF/GCE biosensors. As shown in **Fig. 2A**, no current response was observed among the biosensors in pH 7.4 PBS. However, when 0.5 mM ATCl was added to pH 7.4 PBS, obvious current responses were observed in the five biosensors as shown in **Fig. 2B.** These current responses are attributed to the oxidation of thiocholine, the hydrolysis product of ATCl that is catalyzed by AChE. **Fig. 2B curves a–e** show that the oxidation peak currents increase in an orderly manner and that the oxidation peak potentials shift to lower potentials in sequence. In **Fig. 2B**, curve b was higher than curve a, which is mostly due to the good proton conductivity of NF.[17,23] Incorporation of SNS into the electrode resulted in the higher oxidation peak current and lower oxidation peak potential. CSNS with negative charges can be separated well in NF, resulting in the higher peak signal and lower potential of curve d compared with those

of curve c. Among the five biosensors, the oxidation peak current of curve e was the highest and the oxidation peak potential of curve e was the lowest. These results demonstrate that Pt NPs–CSNS–NF improves the conductivity and catalytic activity of the resulting biosensor. Decreases in the overpotential of thiocholine oxidation help avoid interferences from other electroactive species in a biological matrix.[24–26] The interference of electroactive species will be discussed in detail in the section on interferences.

3.3 Optimization of the preparation of the biosensor

Experiments to determine the optimum volume of Pt NPs–CSNS–NF, ratio of Pt NPs in Pt NPs–CSNS, and pH are described in **Supplementary Materials**.

3.4 Detection of ATCl by NF/AChE–CS/Pt NPs–CSNS–NF/GCE biosensor

The response of the NF/AChE–CS/Pt NPs–CSNS–NF/GCE biosensor to ATCl was explored at the peak potential of 0.55 V according to the optimum conditions. **Fig. 3A** shows the calibration curves for ATCl determination. With increasing ATCl concentration, the amperometric response of the AChE biosensor increased. The amperometric response of the biosensor showed a linear function of ATCl concentration in two segments: from 1 μM to 50 μM and from 50 μM to 500 μM. The detection limit of the biosensor for ATCl was 0.5 μM. When the concentration of

ATCl was saturated, the amperometric response gradually showed a constant value. At higher ATCl concentrations, the shape of the response curve indicated a Michaelis–Menten process (**Fig. 3B**). The K_m^{app} in the present study was calculated as 125 μM according to Eq. 1. This K_m^{app} is lower than those for AChE adsorbed on gold NP/Prussian blue modified electrode (0.30 mM),[27] AChE adsorbed on an NP-SiSG composite film (0.45 mM),[28] and AChE adsorbed on a mesoporous silica-modified electrode (0.38 mM).[29] Because of the excellent electron-transfer channels of Pt NPs–CSNS–NF, the immobilized AChE showed greater affinity and catalytic activity toward ATCl.

3.5 Effect of incubation time

The activity of AChE was influenced by the duration of AChE incubation with 10^{-9} M methyl parathion and carbaryl. The inhibition level of AChE increased with increasing incubation time (**Fig. S2**). Considering the relationship between analytical time and the sensitivity and stability of the current measurements, an exposure time of 10 min was selected as the best compromise between signal and exposure time.

3.6 Detection of pesticides at the NF/AChE–CS/Pt NPs–CSNS–NF/GCE

Inhibition effects by DPV were investigated by measuring the response of the biosensor to 0.5 mM ATCl after incubation with different concentrations of methyl

parathion and carbaryl. **Fig. S3** shows the response of the biosensor before and after 10 min of incubation in 10^{-12}, 10^{-11}, 10^{-10}, 10^{-9}, and 10^{-8} M methyl parathion. The peak currents (**curves b-f**) dramatically decreased compared with that of the control (**curve a**), and the peak current continued to decrease with increasing concentrations of methyl parathion. Calibration plots of inhibition percentage versus pesticide concentration are shown in **Fig. 4**. Linear relationships between the inhibition percentage and the concentration of pesticides were obtained (**Table S1**). The two linear ranges indicate that the biosensor was more sensitive to low concentrations of pesticides than high ones. Comparisons of the analytical performance of the NF/AChE–CS/Pt NPs–CSNS–NF/GCE biosensor in this study and other reported AChE biosensors toward methyl parathion and carbaryl are summarized in **Table 1**. Compared with other biosensors, the present biosensor exhibited lower detection limits and a wider linear range because Pt NPs–CSNS–NF composites increase electrode conductivity, maintain the activity of AChE, and promote electron transfer reactions.

3.7 Interference study

Interference signals from the most common electroactive species are shown in **Fig. S4**. The signal for 0.5 mM ATCl was compared with the signal obtained in the presence of the interfering species after incubated by 10^{-9} M methyl parathion for 10 min. No noticeable changes in current response in the presence of glucose (0.5 mM),

citric acid (0.5 mM), oxalic acid (0.5 mM), PO_4^{3-} (0.5 mM), SO_4^{2-} (0.5 mM), and NO_3^- (0.5 mM) were observed under the present operating potential in this system, which can be attributed to the permselective (charge-exclusion) property of NF films coated on the surface of the biosensor[24] and the low operating potential of the biosensor.[25,26] The negatively charged polymer NF is widely used as a barrier for the diffusion of small neutral or negatively charged interfering species such as ascorbic acid and uric acid. NF is biocompatible with enzymes because it has both hydrophilic and hydrophobic properties. It is chemically inert and exhibits relatively little adsorption of species from the solution. However, 0.5 mM p-nitrophenol, 0.5 mM nitrobenzene, 0.5 mM p-nitroaniline, 0.5 mM trinitrotoluene, 0.5 mM toluene, and 0.5 mM p-toluenesulfonic acid interfered with the determination. Besides, Interferences from other organophosphate and carbamate pesticides such as malathion, acephate, chlorpyrifos, and carbofuran were used to study the interference between the various kinds of pesticides. The results showed malathion, acephate, chlorpyrifos, and carbofuran interfere with the detection of methyl parathion.

3.8 Precision of measurements and stability of the biosensor

The intra-assay precision of the biosensor was evaluated by assaying one enzyme electrode in six-replicate determinations in 0.5 mM ATCl after incubation with 1.0×10^{-10} M methyl parathion for 10 min. In this test, the biosensor was rinsed with 0.1 M PBS and incubated in 0.1 M PBS containing 0.1 mM PAM and 0.1 M PBS

containing 10 mM ATCl for 2 min. The inter-assay precision or fabrication reproducibility was estimated from six different electrodes. The RSD values of intra-assay and inter-assay precisions were 3.2% and 3.6%, respectively, which indicates acceptable reproducibility (**Table. S2**). When the enzyme electrode was not in use, it was stored at 4 °C in a dry environment. No obvious decrease in the current response of ATCl was observed in the first 10 d of storage. After 30 d of storage, the sensor retained 89% of its initial current response, which indicates that the biosensor has acceptable stability (**Fig. S5**). These data suggest that the use of NF polymer as an outer protective layer improves the stability and storage life of the proposed biosensor.

3.9 Analysis of real samples

Spike recovery is useful for investigating the accuracy of an analytical method. A standard addition method was adopted to estimate the accuracy of the proposed biosensor. **Table S3** show the results obtained by analysis of these spiked samples. The recoveries of tap water, lake water, apple, and cabbage were in the range of 93.3%–106.4%, which demonstrates low matrix effects on the current response. The low RSDs for methyl parathion and carbaryl demonstrate the high precision of the proposed biosensor.

In the present work, the Pt NPs–CSNS nanocomposite was homogeneously dispersed in NF and subsequently dropped on the surface of a GCE, forming a

uniform membrane. The Pt NPs–CSNS–NF showed excellent conductivity, biocompatibility, and relatively good catalytic activity, which were attributed to the synergistic effects of Pt NPs, CSNS, and NF. Pt NPs–CSNS–NF/GCE also provided a hydrophilic surface for AChE adhesion. CS was used to immobilize AChE on the surface of Pt NPs–CSNS–NF/GCE, maintain AChE activities, and assist the shuttling of electrons between the enzyme and Pt NPs–CSNS–NF/GCE. Finally, an extra NF coating was used to eliminate common interfering substances and improve the stability of the biosensor.

Many advanced materials have been used in biosensor fabrication to increase the sensitivity of enzyme electrodes. However, the efficient electrical communication between the redox center of the enzyme and solid electrode surfaces remains a challenge to be overcome because the active site of the enzyme is buried deep in the protein shell.[37] Therefore, finding a feasible method by which to further enhance the efficiency of the electrical communication is important. The active site of AChE is located at the bottom of a deep gorge lined largely by aromatic residues. AChE has a strong electrostatic dipole moment.[38] As the axis of the dipole moment of AChE is oriented approximately along the axis of the gorge of the active-site, the dipole moment may attract the positively charged substrate, ATCl, and deactivate the active site.[38]

As shown in **Scheme 1**, alternating positively and negatively charged electrostatic fields were formed by the negatively charged NF, positively charged CS, and negatively charged AChE. Thus, we propose that the alternation of positively and

negatively charged electrostatic fields enhances the electrostatic field strength of the AChE active site and improves the electrochemical response. The enhanced electrochemical response of the NF/AChE–CS/Pt NPs–CSNS–NF/GCE biosensor may be attributed to the improved electron transfer between AChE and the Pt NPs–CSNS–NF nanocomposite-modified electrode. However, whether or not the electron transfer between AChE and biointerface is affected significantly by the alternating positively and negatively charged electrostatic fields is still unknown. Therefore, further study should be done to investigate the electron transfer rate and electrostatic force, both of which are responsible for amplification of electrochemical responses, between AChE and the biointerface. The relationship between structure and specific mechanisms also needs to be studied in detail. Work related to the determination of this relationship is currently in progress in our laboratory.

4. Conclusion

In this work, the advantageous characteristics of Pt NPs, CSNS, CS, and NF are combined in an AChE biosensor. The resulting biosensor exhibited many advantages, including low applied potential, fast response, high sensitivity, acceptable stability, reproducibility, and simple fabrication. The proposed biosensor has potential application in the biomonitoring of methyl parathion and carbaryl pesticides as well as other organophosphate and carbamate pesticides. The biosensor can also be used to immobilize other enzymes to construct a range of biosensors and may be applied in

the assembly of other biological molecules, such as antibodies, antigens, and DNA for wider bioassay applications.

Acknowledgement

This work was supported by the Natural Science Foundation of China (31160334) and the Natural Science Foundation of Yunnan Province (2012FB112), People's Republic of China.

References

1 F. Saez, C. Pozo, M. A. Gomez, M. V. Martinez-Toledo, B. Rodelas, J. Gonzalez-Lopez, *Appl. Microbiol. Biotechnol.*, 2006, 71, 563–567.

2 R. A. Videira, M. C. Madeira, V. I. Lopes, V. M. Madeira, *Biochim. Biophys. Acta*, 2001, **1511**, 360–368.

3 J. M. Gong, X. J. Miao, T. Zhou, L. Z. Zhang, *Talanta*, 2011, **85**, 1344–1349.

4 R. Rawal, S. Chawla, T. Dahiya, C. S. Pundir, *Anal. Bioanal. Chem.*, 2011, **401**, 2599–2608.

5 L. G. Zamfir, L. Rotariu, C. Bala, *Biosens. Bioelectron.*, 2011, **26**, 3692–3695.

6 S. Çevik, S. Timur, Ü. Anik, *Microchim. Acta*, 2012, **179**, 299–305.

7 D. Du, X. X. Ye, J. Cai, J. Liu, A. D. Zhang, Biosens. Bioelectron., 2010, **25**, 2503–2508.

8 C. T. Kresge, M. E. Leonowicz, W. J. Roth, J. C. Vartuli, J. S. Beck, *Nature*, 1992, 359, 710–712.

9 A. Kaushik, P. R. Solanki, K. N. Sood, S. Ahmad, B. D. Malhotra, *Electrochem. Commun.*, 2009, **11**, 1919–1923.

10 X. Y. Zhang, D. X. Liu, D. D. Xu, *Science*, 2012, **29**, 1684–1687.

11 J. Abdullah, M. Ahmad, L. Y. Heng, N. Karuppiah, H. Sidek, *Anal. Bioanal. Chem.*, 2006, **386**, 1285–1292.

12 F. F. Zhang, Q. Wan, C. X. Li, X. L. Wang, Z. Q. Zhu, Y. Z. Xian, L. T. Jin, K. Yamamoto, *Anal. Bioanal. Chem.*, 2004, **380**, 637–642.

13 H. P. Yang, Y. F. Zhu, *Biosens. Bioelectron.*, 2007, **22**, 2989–2993.

14 Y. J. Zou, C. L. Xiang, L. X. Sun, F. Xu, *Biosens. Bioelectron.*, 2008, 23, 1010–1016.

15 L. Bahshi, M. Frasconi, R. Tel-Vered, O. Yehezkeli, I. Willner, *Anal. Chem.*, 2008, **80**, 8253–8259.

16 J. Zhou, J. Y. Zhuang, M. Miró, Z. Q. Gao, G. N. Chen, D. P. Tang, *Biosens. Bioelectron.*, 2012, **35**, 394–400.

17 Z. M. Hu, C. J. Seliskar, W. R. Heineman, *Anal. Chim. Acta*, 1998, **369**, 93–101.

18 A. Kumaravel, M. Chandrasekaran, *J. Electroanal. Chem.*, 2010, **638**, 231–235.

19 J. Li, S. J. Guo, Y. M. Zhai, *Electrochem. Commun.*, 2009, **11**, 1085–1088.

20 M. G. Li, S. D. Xu, M. Tang, *Electrochim. Acta*, 2011, **56**, 1144–1149.

21 A. Sassolas, L. J. Blum, B. D. Leca-Bouvier, *Biotechnol. Adv.*, 2012, **30**, 489–511.

22 Y. Q. An, M. Chen, Q. J. Xue, W. M. Liu, *J. Colloid Interf. Sci.*, 2007, **311**, 507–513.

23 S. Tan, D. Be´langer, *J. Phys. Chem. B*, 2005, **109**, 23480–23490.

24 K. Yang, G. W. She, H. Wang, X. M. Ou, X. H. Zhang, C. S. Lee, S. T. Lee, *J. Phys. Chem. C*, 2009, **113**, 20169–20172.

25 M. H. Yang, Y. H. Yang, Y. Yang, G. L. Shen, Yu RQ, *Anal. Chim. Acta*, 2005, **530**, 205–211.

26 D. Du, J. Wang, J. N. Smith, C. Timchalk, Y. H. Lin, *Anal. Chem.*, 2009, **81**, 9314–9320.

27 S. Wu, X. Q. Lan, W. Zhao, Y. P. Li, L. H. Zhang, H. N. Wang, M. Han, S.Y. Tao,

Biosens. Bioelectron., 2011, **27**, 82–87.

28 D. Du, S. Z. Chen, J. Cai, A. D. Zhang, *Biosens. Bioelectron.*, 2007, **23**, 130–134.

29 S. Wu, L. L. Zhang, L. Qi, S. Y. Tao, X. Q. Lan, Z. G. Liu, C. G. Meng, *Biosens. Bioelectron.*, 2011, **26**, 2864–2869.

30 J. M. Gong, L. Y. Wang, L. Z. Zhang, *Biosens. Bioelectron.*, 2009. **24**, 2285–2288.

31 R. Xue, T. F. Kang, L. P. Lu, S. Y. Cheng, *Appl. Surf. Sci.*, 2012, **258**, 6040–6045.

32 J. M. Gong, Z. Q. Guan, D. D. Song, *Biosens. Bioelectron.*, 2013, **39**, 320–323.

33 Y. P. Li, Y. F. Bai, G. Y. Han, M. Y. Li, *Sens. Actuators, B*, 2013, **185**, 706–712.

34 K. Wang, H. N. Li, J. Wu, C. Ju, J. J. Yan, Q. Liu, B. J. Qiu, *Analyst*, 2011, **136**, 3349–3354.

35 K. Wang, Q. Liu, L. N. Dai, J. J. Yan, C. Ju, B. J. Qiu, X. Y. Wu, *Anal. Chim. Acta*, 2011, **695**, 84–88.

37 H. Zhou, X. Gan, J. Wang, X. L. Zhu, G. X. Li, *Anal. Chem.*, 2005, **77**, 6102–6104.

38 D. R. Ripoll, C. H. Faerman, P. H. Axelsen, I. Silman, J. L. Sussman, *Proc. Natl. Acad. Sci. USA*, 1993, **90**, 5128–5132.

Figure Captions:

Scheme 1. The process of preparation Pt NPs–CSNS–NF nanocomposite and fabrication of the biosensor.

Fig. 1. (A) SEM image of CSNS; (B) SEM image of Pt NPs–CSNS; (C) FTIR spectra of SNS and CSNS; (D) XRD of CSNS and Pt NPs–CSNS.

Fig. 2. CVs of NF/AChE–CS/GCE (a), NF/AChE–CS/NF/GCE (b), NF/AChE–CS/SNS–NF/GCE (c), NF/AChE–CS/CSNS–NF/GCE (d), and NF/AChE–CS/Pt NPs–CSNS–NF/GCE (e) in 0.1 M PBS without (A) and with 0.5 mM ATCl (B). Scan rate: 0.10V/s at 25 ^{o}C.

Fig. 3. (A) The calibration curves for ATCl determination at peak potential of 0.55 V; (B) Lineweaver–Burk plot of $1/i_{ss}$ vs. $1/C$.

Fig. 4. Inhibition curves of NF/AChE–CS/Pt NPs–CSNS–NF/GCE biosensor for methyl parathion and carbaryl determination by DPV. Pulse amplitude: 0.05 V; pulse width: 0.05 s.

Table 1

Comparison of the performance of the biosensor for detection of pesticides with other AChE biosensor.

Sample	Electrode	Liner range (M)	Detection limit (M)	References
MP[a]	AChE–Au–PPy[c]/GCE	1.9×10^{-8} – 4.6×10^{-7}; 1.9×10^{-6} – 1.7×10^{-5}	7.6×10^{-9}	30
	AChE–SF[d]/MWNTs[e]/GCE	3.5×10^{-6} – 2.0×10^{-3}	5.0×10^{-7}	31
	AChE–LDHs[f]/GCE	1.9×10^{-8} – 1.1×10^{-6}; 1.1×10^{-6} – 1.5×10^{-5}	2.3×10^{-9}	32
	NF/AChE–CS/Pt–CSNS–NF/GCE	10^{-13}–10^{-10}; 10^{-10}–10^{-8}	5.52×10^{-13}	This work
CL[b]	AChE–pRGO[g]–CHIT/GCE	5.0×10^{-9} – 2.5×10^{-7}	2.5×10^{-9}	33
	AChE–TiO_2–G[h]/GCE	5.0×10^{-9} – 7.5×10^{-8}; 7.5×10^{-8} – 1.0×10^{-5}	1.5×10^{-9}	34
	AChE–CdS–G[h]–CHIT/GCE	1.0×10^{-8} – 1.0×10^{-5}	3.5×10^{-9}	35
	NF/AChE–CS/Pt–CSNS–NF/GCE	10^{-12}–10^{-10}; 10^{-10}–10^{-8}	5.65×10^{-13}	This work

[a] Methyl parathion.

[b] Carbaryl.

[c] Polypyrrole.

[d] Silk fibroin.

[e] Multiwalled carbon nanotube.

[f] Polyaniline.

[g] Porous-reduced graphene oxide.

[h] Graphene.

Figures:

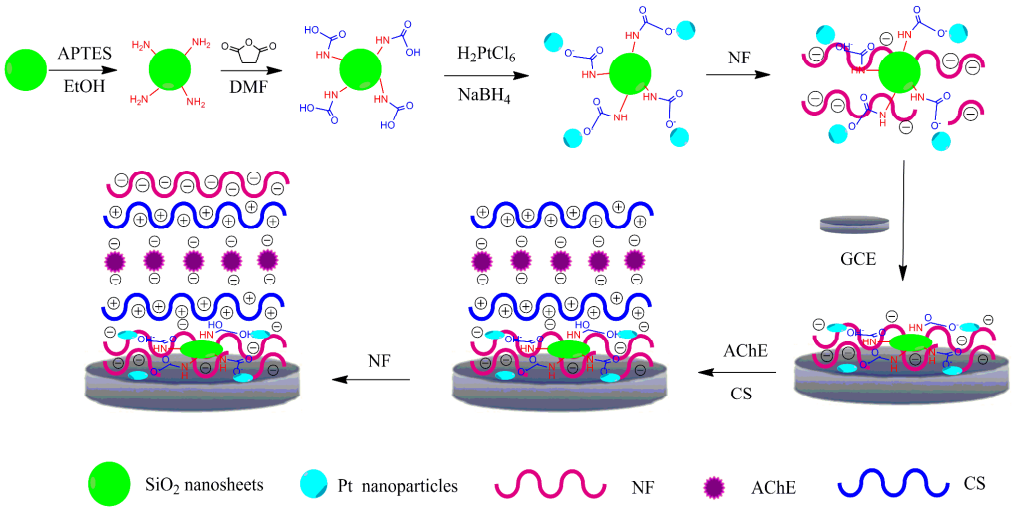

Scheme 1

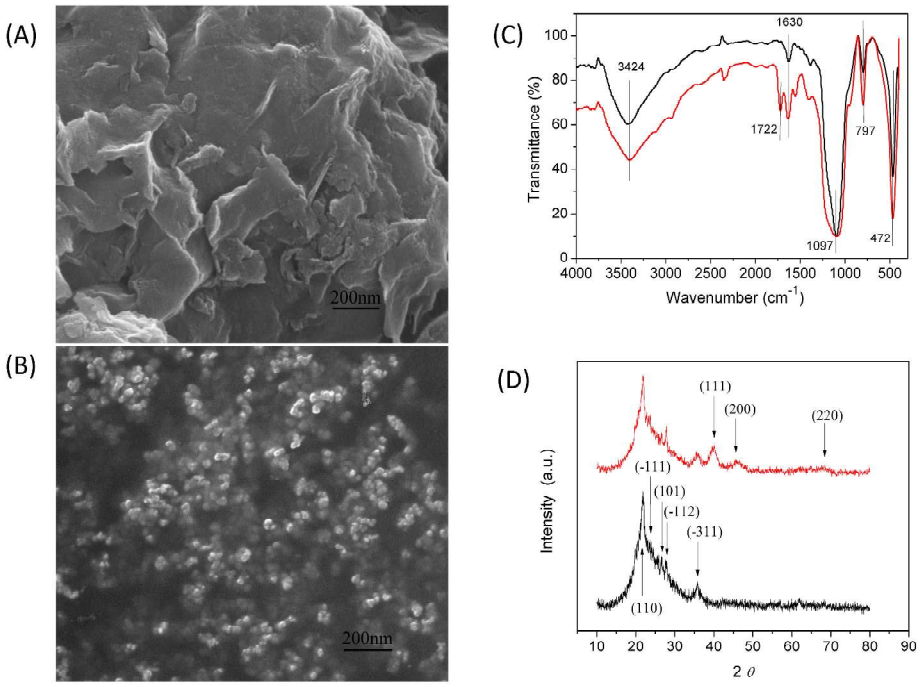

Fig. 1

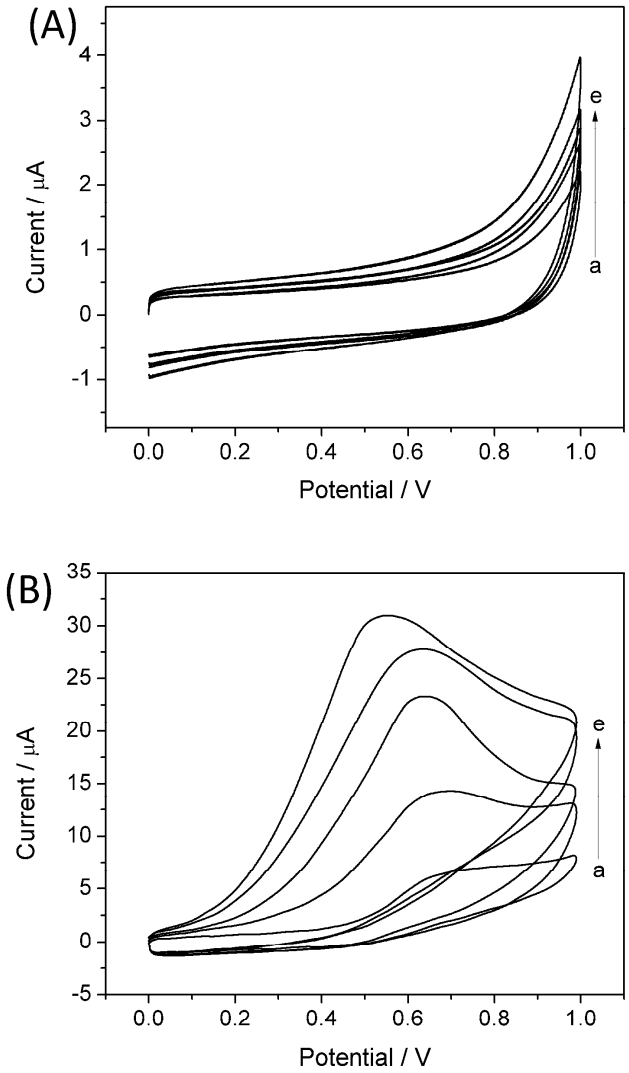

Fig. 2

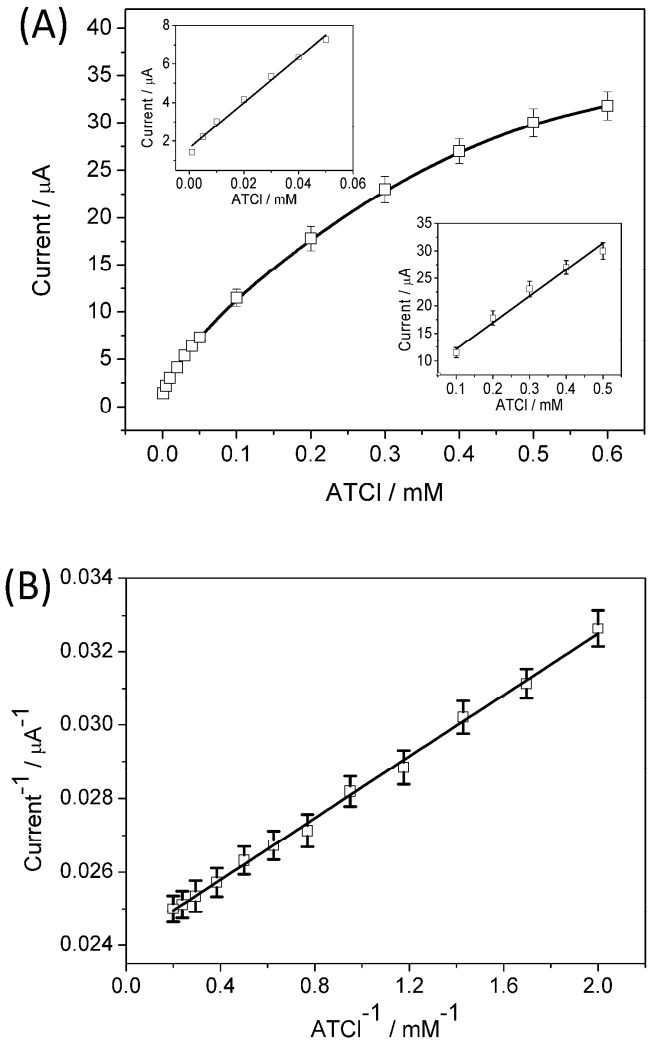

Fig. 3

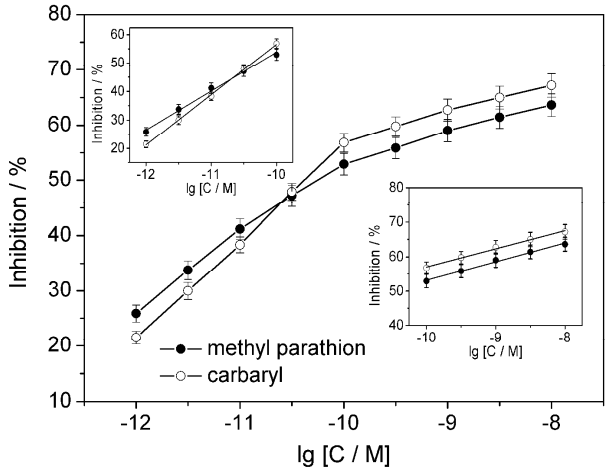

Fig. 4